nature methods

Brief Communication

https://doi.org/10.1038/s41592-023-01911-1

Expansion spatial transcriptomics

Received: 18 October 2022

Accepted: 12 May 2023

Published online: 22 June 2023

Check for updates

Yuhang Fan[1,4], Žaneta Andrusivová[2,4], Yunming Wu[3], Chew Chai[1], Ludvig Larsson[2], Mengxiao He[2], Liqun Luo[3], Joakim Lundeberg[2] ✉ & Bo Wang[1] ✉

Capture array-based spatial transcriptomics methods have been widely used to resolve gene expression in tissues; however, their spatial resolution is limited by the density of the array. Here we present expansion spatial transcriptomics to overcome this limitation by clearing and expanding tissue prior to capturing the entire polyadenylated transcriptome with an enhanced protocol. This approach enables us to achieve higher spatial resolution while retaining high library quality, which we demonstrate using mouse brain samples.

The spatial distribution of transcripts is essential for understanding cell states and cellular organization in tissues. In recent years, many methods for spatial profiling of gene expression have been developed[1–3]. The first technique that can target the entire transcriptome, introduced by Ståhl et al. in 2016 and now commercialized by 10x Genomics as the Visium platform, relies on capturing polyadenylated RNA released from tissue sections onto a barcoded array surface[4]. Its broad applicability has been demonstrated in various systems to describe developmental processes[5] and profile complex diseases[6,7]. However, its spatial resolution is limited by the density of spatially barcoded arrays. Currently, the spot size is 55 µm with a center-to-center distance of 100 µm, resulting in each spot being occupied by multiple cells.

Here we present expansion spatial transcriptomics (Ex-ST), an approach that enables us to overcome the resolution limit by first expanding samples embedded in a polyelectrolyte matrix before capturing RNA on Visium slides. We applied this method on two mouse brain regions, olfactory bulb and hippocampus, chosen for their well-described anatomically distinct patterns with clear molecular signatures. Our Ex-ST protocol significantly improves the resolution and RNA capture efficiency of the Visium array, enabling us to better resolve cell types and detect rare transcripts.

We took inspiration from expansion microscopy, in which biomolecules are anchored to polyelectrolyte gel matrices that can be expanded to increase imaging resolution[8]. In our Ex-ST protocol (Fig. 1a), a tissue section is embedded in a polyacrylate gel to anchor RNA. After all of the proteins are digested, the gel undergoes ~2.5-fold linear expansion in 0.1× SSC (saline-sodium citrate) buffer. The expanded gel is stained with 4,6-diamidino-2-phenylindole (DAPI) and placed on the Visium capture array, where fluorescent images are taken to register nuclei for aligning anatomy and gene expression in later steps. A key design of Ex-ST is the use of two poly-deoxythymidine probes of different lengths and melting temperatures, with the shorter one (melting temperature ~ 39 °C) anchored in the gel and the longer one (melting temperature > 55 °C) spatially barcoded on the Visium slides. This enables us to use heat (45 °C for 30 min) to release RNA molecules from the gel and recapture them on the array surface (Extended Data Fig. 1a–d). Reverse transcription and library preparation were then performed using a modified version of the standard Visium protocol, which enhances RNA capture efficiency with longer capture probes and, thereby, the final library quality (Methods and Extended Data Fig. 1e–g).

We first performed Ex-ST on the mouse olfactory bulb (MOB), in which neurons are organized in spatially distinct laminated zones with well-defined molecular signatures[9,10]. With matched sequencing saturation (Extended Data Table 1), Ex-ST captured more unique molecular identifiers (UMIs) per gene from the same tissue area than the standard Visium protocol (median: Ex-ST, 29.5 ± 2.5; Visium, 14 ± 2; $n = 2$; Fig. 1b), and showed excellent reproducibility between replicates (Extended Data Fig. 2a). As expected, the number of unique molecules and genes detected per spot was lower using Ex-ST, but after normalizing for the tissue area covering each spot, Ex-ST captured more UMIs (median: Ex-ST, 682.5 ± 16; Visium, 503 ± 29; $n = 2$, in areas of 20 µm in diameter; Extended Data Fig. 1g) and unique genes (median: Ex-ST, 430.5 ± 8.5; Visium, 230 ± 21; $n = 2$; Fig. 1c). These observations suggest that Ex-ST achieves higher coverage of transcripts.

To examine any potential bias that may be introduced by the Ex-ST protocol, we first compared gene expression measured by Ex-ST, standard Visium, bulk RNA sequencing (RNA-seq)[11] and Slide-seq[12], and noted

[1]Department of Bioengineering, Stanford University, Stanford, CA, USA. [2]Department of Gene Technology, KTH Royal Institute of Technology, Science for Life Laboratory, Stockholm, Sweden. [3]Department of Biology, Howard Hughes Medical Institute, Stanford University, Stanford, CA, USA. [4]These authors contributed equally: Yuhang Fan, Žaneta Andrusivová. ✉e-mail: joakim.lundeberg@scilifelab.se; wangbo@stanford.edu

https://doi.org/10.1038/s41592-023-01911-1

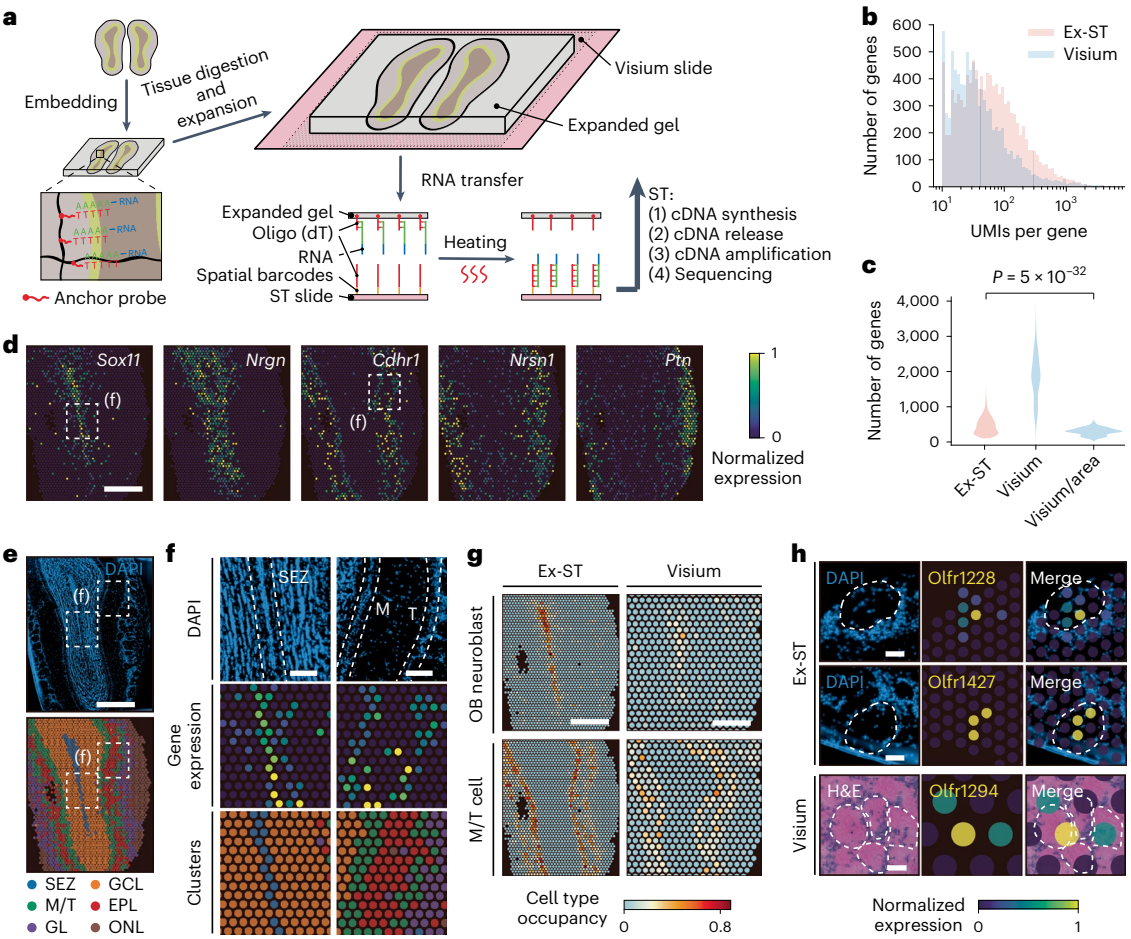

Fig. 1 | Ex-ST resolves MOB layers with high resolution. a, Overview of the Ex-ST workflow. **b**, Comparison of the number of UMIs for all genes present in the Ex-ST and standard Visium datasets, each containing two MOB sections. **c**, Violin plot showing the number of genes per spot measured by Ex-ST, standard Visium, and standard Visium after normalizing for the tissue area covering each spot. *P* value: two-sided, two-sample Mann-Whitney-Wilcoxon test. **d**, Spatially resolved expression of region-specific marker genes processed using the Ex-ST protocol. **e**, DAPI image of an expanded MOB section (top) and annotated clusters on tissue coordinates (bottom): EPL, external plexiform layer; GCL, granular layer; GL, glomerular layer; M/T, mitral and tufted cell layer; ONL, olfactory nerve layer. **f**, Magnified views of the SEZ and M/T regions processed using Ex-ST. Top: DAPI images of the SEZ and M/T regions highlighted with dashed outlines. Middle: expression of region-specific marker genes (*Sox11* for SEZ and *Cdhr1* for M/T region). Bottom: cluster labels mapped on tissue coordinates. **g**, Comparison of cell type occupancy of each spot in the Ex-ST and standard Visium data for two cell types, olfactory bulb (OB) neuroblasts and M/T cells. **h**, Expression of Olfrs in both Ex-ST and standard Visium datasets. DAPI (Ex-ST) and H&E (standard Visium) images showing the locations of glomeruli with boundaries indicated by dashed lines. The localization of Olfr, detected by Ex-ST, in specific glomeruli is in agreement with the coordinates provided by a previous study using serial sectioning[22]. Given that Ex-ST and standard Visium datasets were produced using different MOB specimens, different Olfrs are captured. Scale bars, 500 µm (**d**,**e**,**g**), 100 µm (**f**) and 50 µm (**h**) (scale bars for expanded samples in all panels have been rescaled by the expansion ratio).

broad agreement between methods (Extended Data Fig. 2b–d). Furthermore, this is supported by the similar RNA biotype composition, 3′ bias in gene body coverage, and the size distribution of captured transcripts between Ex-ST and standard Visium (Extended Data Fig. 2e–g). We also noted that Ex-ST captured more intronic reads, potentially due to the protocol modifications and protein digestion step that better exposed the nuclear RNA (Extended Data Fig. 2h).

The spatial distribution of region-specific marker genes, including *Sox11* for the subependymal zone (SEZ), *Nrgn* for the granular layer, *Cdhr1* for the mitral and tufted cell layers, *Nrsn1* for the glomerular layer and *Ptn* for the olfactory nerve layer[9], showed expected layered patterns (Fig. 1d and Extended Data Fig. 3a)[10], and indeed had higher UMI counts than in the standard Visium protocol (Extended Data Fig. 3b). By clustering the Ex-ST data, we identified six clusters, each corresponding to a morphological layer of MOB, and annotated them based on their marker genes and spatial locations (Fig. 1e and Extended Data Fig. 3c–e). In particular, the SEZ and the mitral and tufted clusters covered only 1–2 lines of spots, consistent with the width (<50 µm) of these layers (Fig. 1f).

We next determined whether tissue expansion reduced the number of cells occupying each spot. We applied stereoscope, a deconvolution algorithm to infer cell type composition of each spot using single-cell transcriptomes[13]. We observed that Ex-ST data contained more spots with a single dominant cell type than both the standard and modified Visium protocols (Extended Data Fig. 4). For example, the SEZ and the mitral–tufted regions had 16 and 96 spots, respectively, in which the occupancy of a single cell type was >50%, with the highest values reaching ~80%. In contrast, standard Visium data had no spots in SEZ and only two in the mitral–tufted region, with dominating cell type occupancy barely over 50%, suggesting that Ex-ST can better separate cell types in space (Fig. 1g).

Encouraged by the enhanced resolution of Ex-ST, we examined the glomeruli in olfactory bulbs, the size of which ranges between 50 µm and 120 µm in diameter. Consequently, the resolution of gene

https://doi.org/10.1038/s41592-023-01911-1

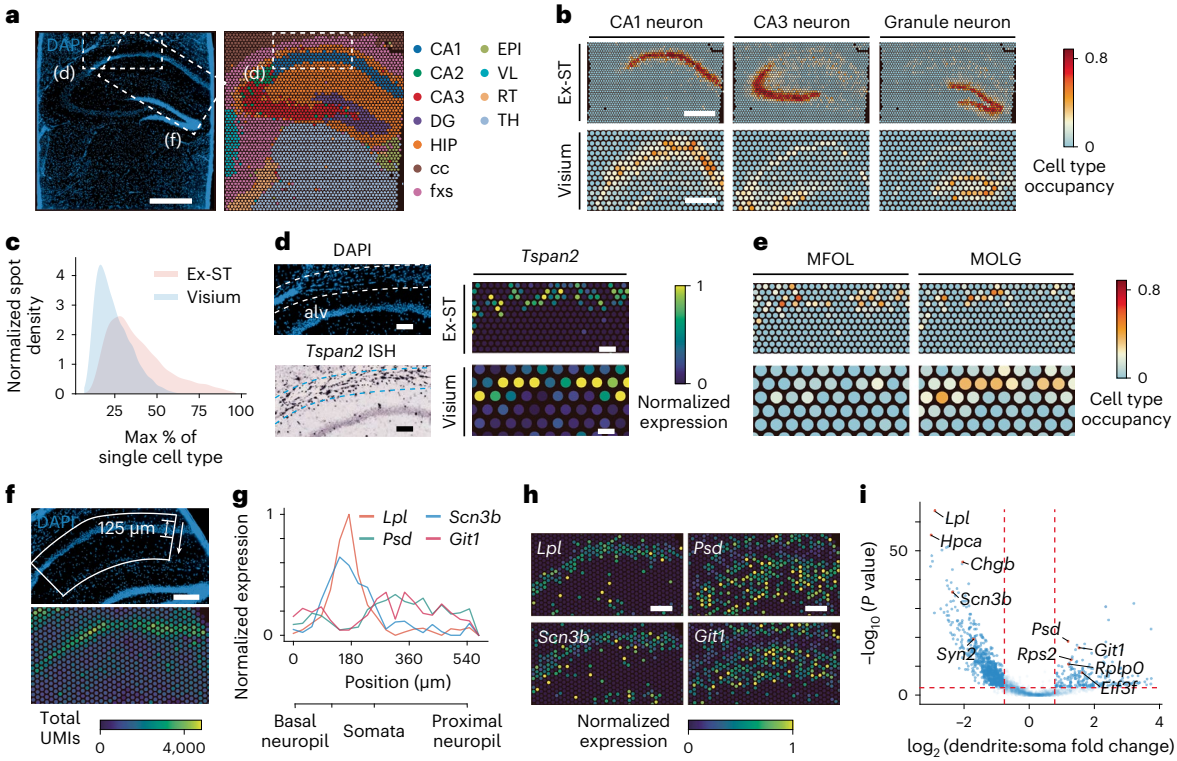

Fig. 2 | Ex-ST dissects fine structures in the mouse hippocampus. a, DAPI image of an expanded mouse hippocampus section (left) and annotated clusters on tissue coordinates (right): CA (cornu ammonis) 1–3, hippocampal subfields; cc, corpus callosum; DG, dentate gyrus; EPI, epithalamus; fxs, fornix system; HIP, hippocampal region; RT, reticular nucleus of the thalamus; TH, thalamus; VL, lateral ventricle. **b**, Comparison of cell type composition of individual spots in the Ex-ST and standard Visium data for three cell types. **c**, Occupancy of the dominant cell type in each spot for both the Ex-ST and standard Visium data, presented as a density plot. **d**, Top left: magnified DAPI image showing the sporadic distribution of cell bodies in the alveus (alv, dashed outlines). Bottom left: in situ hybridization (ISH) of *Tspan2* showing oligodendrocyte cell bodies, obtained from the Allen brain atlas[10]. Right: comparison of normalized *Tspan2* expression in the Ex-ST and standard Visium data. **e**, Comparison of cell type composition of individual spots in the Ex-ST and standard Visium data for oligodendrocyte subclasses (MFOL, myelin-forming oligodendrocyte; MOLG, mature oligodendrocyte). **f**, Top: magnified DAPI image showing the high nuclear density in the CA1 region. Bottom: spatial distribution of UMI counts in the CA1 region. **g**, Expression profiles of soma–dendrite differentially expressed genes along the axis indicated by the arrow in **f**. **h**, Normalized spatial expression of soma-enriched (left column) and dendrite-enriched (right column) genes. **i**, Volcano plot showing differential gene expression between soma and dendritic regions. *P* values: two-sided, two-sample Mann-Whitney-Wilcoxon tests. Genes with $\log_2$ (fold change) > 0.8 and $P < 0.001$ (dashed lines) are considered differentially expressed. Several previously known soma- and dendrite-enriched genes are specified. Scale bars, 500 µm (**a**,**b**), 100 µm (**d**) and 200 µm (**f**,**h**) (scale bars for expanded samples in all panels have been rescaled by the expansion ratio).

expression in individual glomeruli using standard Visium is challenging. In contrast, Ex-ST enabled us to map olfactory receptors (Olfrs) directly onto single glomeruli (Fig. 1h), consistent with previous findings that olfactory sensory neurons projecting their axons into a common glomerulus should express the same type of Olfr[14,15]. This demonstrates the potential of Ex-ST to elucidate tissue organization at a finer scale.

Applying Ex-ST to mouse hippocampus, we identified 11 clusters corresponding to different anatomical regions, expressing known marker genes (Fig. 2a and Extended Data Fig. 5a–c), while the expression levels, 3′ bias and RNA biotype composition are largely consistent between Ex-ST and standard Visium (Extended Data Fig. 5d–h). Stereoscope analysis showed that most spots in the cornu ammonis and dentate gyrus regions had occupancy by a single cell type of >80%, whereas the standard Visium data rarely had spots with cell type occupancy over 50% (Fig. 2b and Extended Data Fig. 6a). Overall, Ex-ST shifted the cell type composition per spot towards single cell type occupancy throughout the hippocampus (Fig. 2c).

Notably, by expanding the tissue, we resolved subclasses of oligodendrocytes in the alveus, a dense layer of myelinated axonal fibers covering the ventricular parts of the hippocampus. Consistent with in situ hybridization, oligodendrocyte markers, such as *Tspan2*, were distributed sporadically in this layer in our Ex-ST data, whereas their expression in the standard Visium data was more continuous and diffusive (Fig. 2d and Extended Data Fig. 6b). Deconvolving the expression of individual spots using stereoscope showed the distinct patterns of several oligodendrocyte subtypes in the Ex-ST data, including myelin-forming oligodendrocyte and mature oligodendrocyte[16], which were mixed in the standard Visium data (Fig. 2e and Extended Data Fig. 6c). This suggests that Ex-ST improves the capacity for distinguishing spatially mixed sub-cell types that are only subtly different.

Last, we showed that Ex-ST could measure the subcellular distribution of transcripts. Although most neurons have more transcripts in somata, cornu ammonis-1 neurons actively transport specific transcripts to dendrites[17]. Indeed, the total number of UMIs decreased from the somata into the stratum radiatum in a distance matching the expected size of somata (~125 µm) (Fig. 2f), suggesting that the lateral diffusion of transcripts during RNA capture is negligible. With higher spatial resolution, Ex-ST was able to resolve differentially located transcripts in somata and dendrites, including dendrite-enriched genes such as *Psd* and *Git1* (Fig. 2g,h). Through differential gene expression analysis and after the removal of glial transcripts, Ex-ST identified ~500 dendrite-enriched genes that were unresolvable with the standard Visium protocol, all of which overlapped with at least one of the three

previous studies using orthogonal methods to identify dendritic transcripts in cornu ammonis neurons (Fig. 2i, Extended Data Fig. 6d and Extended Data Table 2)[18–20].

In summary, Ex-ST overcomes the density limitation of spatially barcoded capture arrays by expanding the polyelectrolyte gels to which RNA molecules are anchored. The advances made in this study are in two major areas. First, enlarged biological structures cover more capture spots, which extends the spatial resolution of the Visium array from 55 µm to 20 µm. Second, optimization of RNA capture is crucial for Ex-ST because it enables the detection of more transcripts from fewer cells per spot. Although the gel embedding and expansion steps take additional processing time (~3 days) compared with the standard Visium protocol, Ex-ST does not require the specialized equipment needed in imaging-based in situ sequencing methods (see Supplementary Discussion for further comparisons between Ex-ST and other high-resolution spatial transcriptomics techniques). Finally, our approach is orthogonal to other method development efforts in the field that have primarily focused on shrinking the capture spot size[2,3,18,21], and therefore it has the potential to be integrated with other techniques to enhance their performance as well.

Online content

Any methods, additional references, Nature Portfolio reporting summaries, source data, extended data, supplementary information, acknowledgements, peer review information; details of author contributions and competing interests; and statements of data and code availability are available at https://doi.org/10.1038/s41592-023-01911-1.

References

1. Larsson, L., Frisén, J. & Lundeberg, J. Spatially resolved transcriptomics adds a new dimension to genomics. *Nat. Methods* **18**, 15–18 (2021).
2. Rao, A., Barkley, D., França, G. S. & Yanai, I. Exploring tissue architecture using spatial transcriptomics. *Nature* **596**, 211–220 (2021).
3. Moses, L. & Pachter, L. Museum of spatial transcriptomics. *Nat. Methods* **19**, 534–546 (2022).
4. Ståhl, P. L. et al. Visualization and analysis of gene expression in tissue sections by spatial transcriptomics. *Science* **353**, 78–82 (2016).
5. Asp, M. et al. A spatiotemporal organ-wide gene expression and cell atlas of the developing human heart. *Cell* **179**, 1647–1660 (2019).
6. Lewis, S. M. et al. Spatial omics and multiplexed imaging to explore cancer biology. *Nat. Methods* **18**, 997–1012 (2021).
7. Maniatis, S. et al. Spatiotemporal dynamics of molecular pathology in amyotrophic lateral sclerosis. *Science* **364**, 89–93 (2019).
8. Wassie, A. T., Zhao, Y. & Boyden, E. S. Expansion microscopy: principles and uses in biological research. *Nat. Methods* **16**, 33–41 (2019).
9. Tepe, B. et al. Single-cell RNA-seq of mouse olfactory bulb reveals cellular heterogeneity and activity-dependent molecular census of adult-born neurons. *Cell Rep.* **25**, 2689–2703 (2018).
10. Allen Institute for Brain Science. *Allen Mouse Brain Atlas*. mouse.brain-map.org (2004).
11. Endo, F. et al. Molecular basis of astrocyte diversity and morphology across the CNS in health and disease. *Science* **378**, eadc9020 (2022).
12. Rodriques, S. G. et al. Slide-seq: a scalable technology for measuring genome-wide expression at high spatial resolution. *Science* **363**, 1463–1467 (2019).
13. Andersson, A. et al. Single-cell and spatial transcriptomics enables probabilistic inference of cell type topography. *Commun. Biol.* **3**, 565 (2020).
14. Ressler, K. J., Sullivan, S. L. & Buck, L. B. Information coding in the olfactory system: evidence for a stereotyped and highly organized epitope map in the olfactory bulb. *Cell* **79**, 1245–1255 (1994).
15. Vassar, R. et al. Topographic organization of sensory projections to the olfactory bulb. *Cell* **79**, 981–991 (1994).
16. Zeisel, A. et al. Molecular architecture of the mouse nervous system. *Cell* **174**, 999–1014 (2018).
17. Kosik, K. S. Life at low copy number: how dendrites manage with so few mRNAs. *Neuron* **92**, 1168–1180 (2016).
18. Stickels, R. R. et al. Highly sensitive spatial transcriptomics at near-cellular resolution with Slide-seqV2. *Nat. Biotechnol.* **39**, 313–319 (2021).
19. Tushev, G. et al. Alternative 3′ UTRs modify the localization, regulatory potential, stability, and plasticity of mRNAs in neuronal compartments. *Neuron* **98**, 495–511 (2018).
20. Ainsley, J. A., Drane, L., Jacobs, J., Kittelberger, K. A. & Reijmers, L. G. Functionally diverse dendritic mRNAs rapidly associate with ribosomes following a novel experience. *Nat. Commun.* **5**, 4510 (2014).
21. Chen, A. et al. Spatiotemporal transcriptomic atlas of mouse organogenesis using DNA nanoball-patterned arrays. *Cell* **185**, 1777–1792 (2022).
22. Zhu, K. W. et al. Decoding the olfactory map through targeted transcriptomics links murine olfactory receptors to glomeruli. *Nat. Commun.* **13**, 5137 (2022).

https://doi.org/10.1038/s41592-023-01911-1

Methods

Animals

Adult male CD1 mice (3–6 months old, Charles River) were used for the Ex-ST experiments. Animal procedures were approved by the Stanford University Animal Care and Use Committee and were in accordance with National Institutes of Health guidelines. Animals were maintained in a 12 h light–dark cycle, with ambient temperature between 71 °F and 74 °F (21–23 °C), humidity between 20% and 45%, and food and water provided ad libitum. MOB samples for the standard Visium experiment were commercially purchased from Adlego Biomedical, which operates under ethics permission no. 17114–2020.

Tissue preparation

Animals were euthanized with CO_2 followed by cervical dislocation. Brain tissue was quickly dissected and embedded in OCT (Tissue tek, cat. no. 981385). The tissue block was snap-frozen using liquid nitrogen vapor until the OCT block was hardened, and then stored at −80 °C until use. Tissues were cryosectioned to a thickness of 15 µm on a Leica cryostat and placed onto charged glass slides (VWR, cat. no. 75799).

Visium slides for Ex-ST

Ex-ST used multimodal spatial arrays. Each capture area has dimensions of 6.5 × 6.5 mm and contains 5,000 spots of 55 µm in diameter. Surface capture probes include spatial barcodes, UMIs and a 50 TVN sequence to enable polyadenosine-mediated capture of RNA molecules.

Expansion

All steps prior to reverse transcription were performed on charged glass slides (VWR). This eliminates the difficult task of placing tissue sections into the Visium capture area, which can result in failed positioning or tissue folding requiring a slide reset. Sections were fixed with acetone for 1 h at −20 °C, followed by incubation in the hybridization buffer, containing 1 µM anchor probe[23] (a 15-nucleotide sequence of alternating dT and thymidine-locked nucleic acid (dT+) with a 5′-acrydite modification, Integrated DNA Technologies), 2× SSC, 30% [v/v] formamide (Millipore Sigma, cat. no. 11814320001), 0.1% [w/v] yeast transfer RNA (Calbiochem, cat. no. 55714), 1% [v/v] RNase inhibitor (Promega, cat. no. N2615), and 10% [w/v] dextran sulfate (Sigma, cat. no. D8906), at 37 °C under saturation humidity for 40 h. After anchor probe hybridization, sections were washed three times with 1× SSC.

The expansion protocol followed a sequence of gelation, proteinase K digestion, and expansion, as previously described[24]. In brief, samples were washed three times in PBS, then incubated in the monomer solution (1× PBS, 2 M NaCl, 8.625% [w/w] sodium acrylate, 2.5% [w/w] acrylamide, 0.15% [w/w] N,N′-methylenebisacrylamide) for 45 min at 4 °C. Gelation was initiated by adding 0.2% [w/v] ammonium persulfate (ThermoFisher Scientific, cat. no. 17874), 0.01% [w/w] 4-hydroxy-2,2,6,6-tetramethylpiperidin-1-oxyl (4-hydroxy-TEMPO, Sigma-Aldrich, cat. no. 176141) and 0.2% [w/w] tetramethylethylenediamine (ThermoFisher Scientific, cat. no. 17919). The gelation step was performed at 37 °C for 1–2 h.

After gelation, samples were gently removed from the chamber and digested overnight at 37 °C in 8 U ml^{-1} proteinase K (NEB, cat. no. P8107) in digestion buffer (1× TAE buffer, 0.5% Triton X-100, 0.8 M guanidine HCl). Gels were then removed from the digestion buffer and placed in 0.1× SSC to expand. The 0.1× SSC was exchanged every 15 min for 3–5 times until the gel size plateaued. To stain nuclei, expanded samples were incubated with 100 µM DAPI in 0.1× SSC for 30 min. Both bright field and DAPI images of expanded samples were taken after the gel was placed on top of the Visium array and prior to RNA release and reverse transcription.

Ex-ST library preparation

First, to determine the optimal temperature for RNA release from the gel, several temperatures were tested. We analyzed the released RNAs using a bioanalyzer (Agilent 2100) to measure the concentration and length distribution (Extended Data Fig. 1a). We observed that RNA molecules were released from the gel with high integrity as long as the temperature exceeded 41 °C (Extended Data Fig. 1b–d). No significant differences were noted in the released RNA concentration between 41 °C and 45 °C (Extended Data Fig. 1d) and therefore we chose to perform the experiment at 45 °C for 30 min to ensure that RNA molecules are fully released from the gel and to prevent re-hybridization with anchor probes.

Reverse transcription was modified from the standard protocol and conducted at 42 °C for 60 min followed by 53 °C for 45 min using the Visium Spatial Gene Expression reagents (10x Genomics). This extended time of reverse transcription was chosen to enhance the reaction efficiency. After reverse transcription, the second strand synthesis was performed according to the 10x Genomics Visium Spatial Gene Expression protocol, followed by quantitative polymerase chain reaction to determine the number of amplification cycles. An extra polymerase chain reaction cycle was added in the amplification step, in addition to the recommended number of cycles in the Visium Gene Expression protocol. A higher concentration of SPRIselect beads (0.8-fold, instead of 0.6-fold in the standard Visium protocol) was used in the post-amplification clean-up step to retain more fragments. The rest of the library preparation was carried out according to the 10x Genomics Visium Spatial Gene Expression protocol (User Guide CG000239_RevF). Finished libraries were sequenced on a NextSeq 2000 platform (Illumina).

To quantify how these protocol modifications and longer surface probes may affect RNA capture efficiency, we applied the modified protocols (without expansion) on MOB sections of 15 µm in thickness, matching the tissue sections used for the Ex-ST experiments. This experiment generated libraries with high complexity, leading to low sequencing saturation (~60%) even with high numbers of sequencing reads per spot (Extended Data Table 1). For fair comparison, we downsampled the Ex-ST and standard Visium datasets using Seqtk v1.3 to match the sequencing saturation across experiments. We found that, compared with the standard Visium protocol, the modified protocol detected a higher number of UMIs per gene (mean: standard Visium, 38.5 ± 5.5; modified Visium, 538 ± 13; $n = 2$) and number of genes per tissue area (mean: standard Visium, 163.5 ± 14.5; modified Visium, 1,270.5 ± 5.5; $n = 2$) (Extended Data Fig. 1e–g). Given that incomplete poly-deoxythymidine probe hybridization, tissue digestion and gel expansion may result in transcript loss, these modifications are crucial for the implementation of Ex-ST because they enable the detection of more transcripts from fewer cells compared with the standard Visium protocol (Extended Data Fig. 1e–g).

Image acquisition and processing

Bright field and DAPI images of expanded samples were taken on a Zeiss Axio Observer Z1 inverted microscope equipped with an Axiocam 503M camera and a ×5/0.25 objective using Zen Pro 2012 software. The imaging time was minimized to prevent gel from drying and shrinking. The bright field image of the array frame and gel position in each capture area was aligned with the corresponding DAPI image. Manual selection of spots under the tissue was done using Loupe Browser (v4.0.0, 10x Genomics).

Standard Visium library preparation of mouse olfactory bulb

The fresh-frozen MOB sample was cryosectioned at a thickness of 10 µm, placed onto Visium glass slides and stored at −80 °C prior to processing. The spatial gene expression libraries were prepared according to the manufacturer's protocol (Visium Spatial Gene Expression, User Guide CG000239_RevC). Finished libraries were sequenced on a NextSeq 2000 platform (Illumina).

Data processing

The MOB data generated by the standard Visium protocol were processed using space ranger software (v1.0.0, 10x Genomics).

All Ex-ST data were processed using space ranger software (v1.3.0, adapted to work with custom barcode list, 10x Genomics). Reads were aligned to the pre-built mouse reference genome (mm10, 10x Genomics). Processed output files for the standard Visium data of the coronal mouse brain section containing the hippocampus region were downloaded from the 10x Genomics website.

Data analysis

Analysis of data generated by both Ex-ST and standard Visium was performed in Python v3.7.12 and R v4.0.5. Spots with fewer than 100 genes detected (UMI > 1) were excluded from the analysis. For plotting of spatial gene expression and analysis of differential gene expression, expression at each spot was normalized using Scanpy v1.8.2 to the same total count. Dimensional reduction and clustering were performed using the self-assembling manifolds algorithm (v0.8.9) (ref. 25) with default parameters. Spot deconvolution analysis was performed using stereoscope[13]. The mouse brain single-cell RNA-seq data used for deconvolution was the 'Adolescent mouse brain' dataset obtained from http://mousebrain.org/. Spatial plots for cell type mapping were produced in R v4.0.5 using the Seurat (v4.1.1) and STUtility (v0.1.0) R packages. Cornu ammonis-1 soma and dendrite regions used for differential gene expression analysis were selected manually based on the DAPI images.

To examine whether sequencing saturation affects spot devolution analysis and dendritic gene discovery, we downsampled the Ex-ST data using Seqtk v1.3 to match the lower sequencing saturation of the 10x Genomics mouse hippocampus dataset. After downsampling, spots in the major hippocampal regions, including the cornu ammonis and dentate gyrus, still had single cell type occupancy greater than 80% (Extended Data Fig. 6a). We were still able to resolve distinct patterns of oligodendrocyte subtypes (Extended Data Fig. 6c) and identify more than 90% of dendrite-enriched genes, which were undetected using the standard Visium protocol (Extended Data Table 2).

Statistics and reproducibility

P values were calculated using the Mann-Whitney-Wilcoxon test or Welch's *t*-test as indicated using the sciPy library (v1.9.1) with the default parameters. Gene expression profiles along the soma–dendrite axis were generated by averaging the expression of spots at the same distance from the soma region. All spatial profiles of gene expression, cluster annotation and cell type occupancy shown in this study are representative images from two independent replicates.

Reporting summary

Further information on research design is available in the Nature Portfolio Reporting Summary linked to this article.

Data availability

Mouse brain section containing the hippocampus region is a publicly available dataset that can be found (along with the mouse reference genome mm10) on the 10x Genomics website (https://www.10xgenomics.com/resources/datasets/mouse-brain-section-coronal-1-standard-1-0-0). The single-cell RNA-seq dataset of mouse brain can be downloaded online (http://mousebrain.org/adolescent/downloads.html). Mouse olfactory bulb (MOB) bulk RNA-seq and Slide-seq datasets used for comparison were obtained from refs. 11,12. All data generated in this study (standard Visium data on MOB, all Ex-ST data and Visium data generated using the modified protocol) including space ranger output files, stereoscope output files, DAPI and bright field images are available at the Mendeley repository[26]. Raw sequence data can be found at the NCBI BioProject with the accession number PRJNA957091. Source data are provided with this paper.

Code availability

The code used for data analysis and generating figures is available at https://github.com/fyh1221/Expansion_Spatial_Transcriptomics.

References

23. Moffitt, J. R. et al. High-performance multiplexed fluorescence in situ hybridization in culture and tissue with matrix imprinting and clearing. *Proc. Natl Acad. Sci. USA* **113**, 14456–14461 (2016).
24. Fan, Y. et al. Mechanical expansion microscopy. *Methods Cell Biol.* **161**, 125–146 (2021).
25. Tarashansky, A. J., Xue, Y., Li, P., Quake, S. R. & Wang, B. Self-assembling manifolds in single-cell RNA sequencing data. *eLife* **8**, e48994 (2019).
26. Andrusivova, Z. & Fan, Y. Ex-ST, *Mendeley Data*, **v1**, https://doi.org/10.17632/nrbsxrk9mp.1

Acknowledgements

We thank Y. Lim, J. Gibson and Z. Zeng for critical discussions, and K. Zhu and H. Matsunami for sharing the data to validate the mapped glomeruli positions. Y.F. is a Bio-X Stanford Interdisciplinary Graduate Fellow. C.C. is supported by an NSF Graduate Research Fellowship and a Stanford Graduate Fellowship. B.W. is a Beckman Young Investigator. This work is supported by an National Institutes of Health grant (1R35GM138061) to B.W., the Neuro-omics project of Wu Tsai Big Ideas in Neuroscience program to L.Lu. and B.W., the European Research Council (ERC) under the European Union's Horizon 2020 research and innovation program (grant agreement no. 101021019) to J.L., and a Swedish Research Council grant to J.L.

Author contributions

Y.F., Ž.A., J.L. and B.W. initiated and designed the project; Y.F., Ž.A., Y.W. and C.C. performed the experiments; Y.F. and Ž.A. analyzed the data with assistance from Y.W., L.La. and M.H.; Y.F., Ž.A. and B.W. wrote the paper with input from all of the other authors; L.Lu., J.L. and B.W. provided supervision and guidance.

Competing interests

Ž.A., L.La., M.H. and J.L. are scientific consultants for 10x Genomics, which holds intellectual property rights to the spatial transcriptomics technology. The other authors declare no competing interests.

Additional information

Extended data are available for this paper at https://doi.org/10.1038/s41592-023-01911-1.

Supplementary information The online version contains supplementary material available at https://doi.org/10.1038/s41592-023-01911-1.

Correspondence and requests for materials should be addressed to Joakim Lundeberg or Bo Wang.

Peer review information *Nature Methods* thanks Iwijn De Vlaminck, Chenglong Xia, and the other, anonymous, reviewer(s) for their contribution to the peer review of this work. Peer reviewer reports are available. Primary Handling Editor: Rita Strack, in collaboration with the *Nature Methods* team.

https://doi.org/10.1038/s41592-023-01911-1

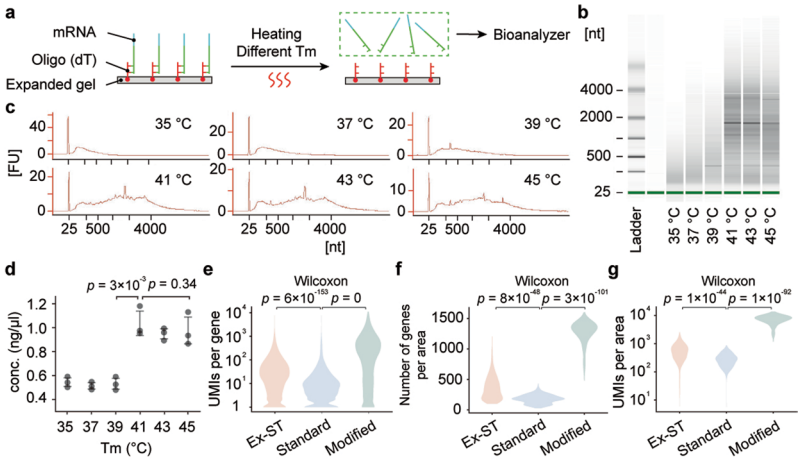

Extended Data Fig. 1 | RNA release and capture. a, The workflow to identify the optimal release temperature. Gel with anchored transcripts was heated for 30 min at different temperatures to release RNA molecules, which were collected and quantified on a Bioanalyzer. b, Representative bioanalyzer gel image from three replicates, showing RNA released from the gel at different incubation temperatures. c, Representative bioanalyzer traces showing the released RNA. Only weak rRNA peaks are expected as the RNA anchoring is mediated by polyA. d, Released RNA concentrations at different incubation temperatures measured from three biological replicates. Error bars: mean ± standard derivation (SD). Increasing temperature from 39 °C to 41 °C significantly increased RNA concentrations, whereas no significant difference was observed above 41 °C. *P* values: two-sided Welch's t-test. e, Violin plot showing the number of UMIs per gene detected by Ex-ST and Visium using standard and modified protocols. f-g, Comparisons of number of genes (f) and UMIs (g) per tissue area (20 by 20 µm) measured by Ex-ST and Visium using the standard and modified protocols, calculated by normalizing the number of genes and UMIs per spot by the tissue area covering each spot. Ex-ST and standard Visium data in e-g were downsampled to match sequencing saturation (Extended Data Table 1). *P* values: two-sided, two-sample Mann-Whitney-Wilcoxon tests.

https://doi.org/10.1038/s41592-023-01911-1

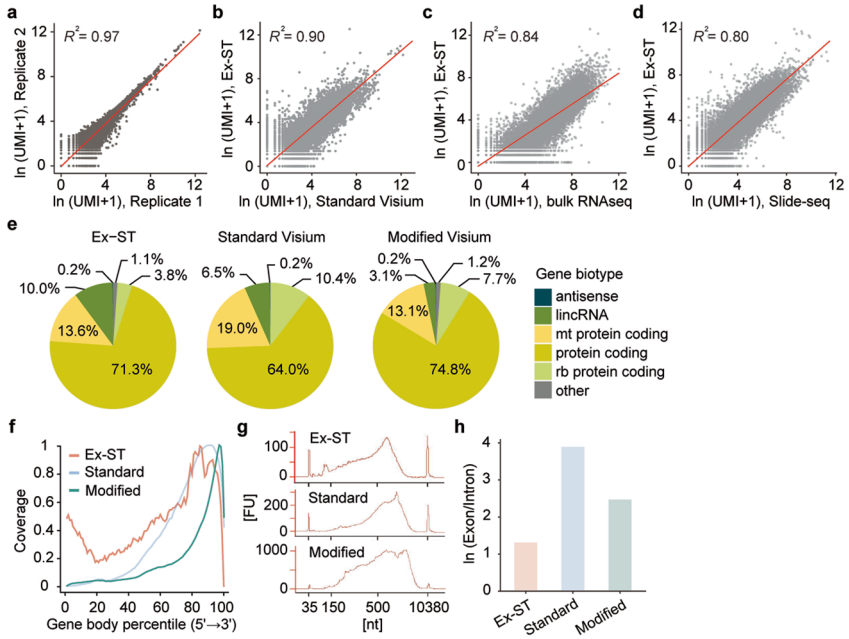

Extended Data Fig. 2 | Ex-ST captures RNA with limited biases. a, Comparison of the number of UMIs per gene between two Ex-ST MOB replicates. **b-d**, Comparisons of the number of UMIs per gene detected in the Ex-ST and standard Visium MOB datasets (**b**), in the Ex-ST and bulk RNA-seq MOB datasets (**c**) and in the Ex-ST and Slide-seq hippocampus datasets (**d**). Red lines: least squares linear fit. **e**, Pie charts showing RNA biotypes captured by Ex-ST and Visium using standard and modified protocols from MOB samples. Proportions are quantified by the total UMI counts of each biotype. **f**, Gene body coverage for the Ex-ST and standard/modified Visium MOB data. **g**, Bioanalyzer traces of cDNA from MOB samples before the fragmentation step for the Ex-ST and standard/modified Visium protocols. **h**, Ratio of exonic and intronic reads in the Ex-ST and standard/modified Visium MOB data.

https://doi.org/10.1038/s41592-023-01911-1

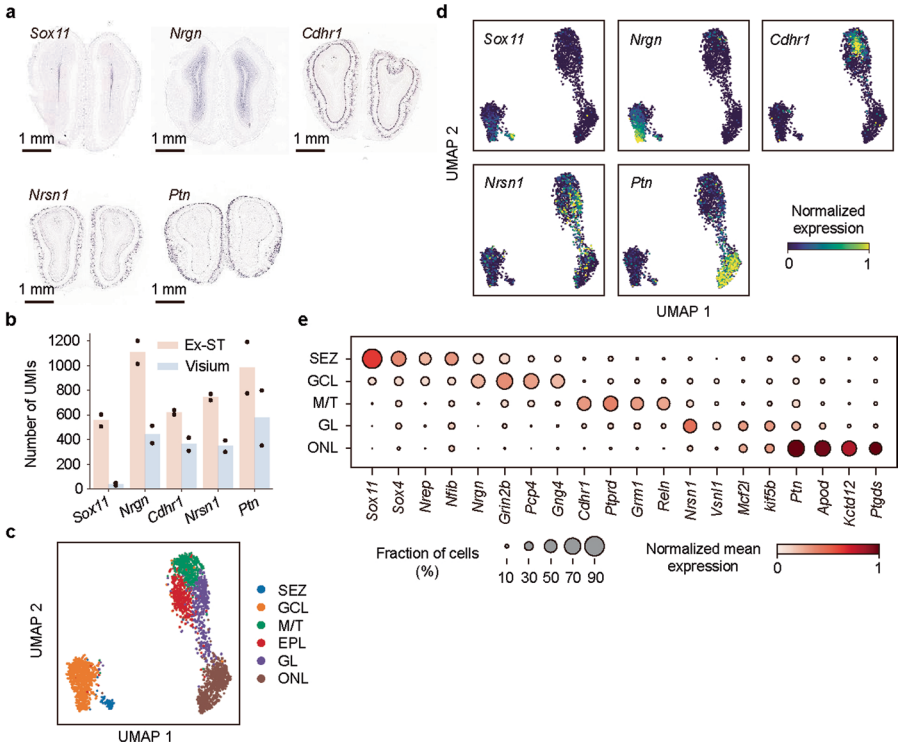

Extended Data Fig. 3 | Annotation of spatial clusters of the MOB Ex-ST data. a, The expression of region-specific marker genes detected by ISH, obtained from Allen Brain Atlas[10]. **b**, Comparison of number of UMIs of select region-specific marker genes measured by Ex-ST and standard Visium from matched tissue areas. Bar charts: mean of two replicates. **c**, UMAP showing Ex-ST MOB clusters identified by unsupervised clustering, colored by cluster annotation. **d**, Marker gene expression overlaid on the UMAP visualization. **e**, Dot plot showing top marker genes for each cluster.

https://doi.org/10.1038/s41592-023-01911-1

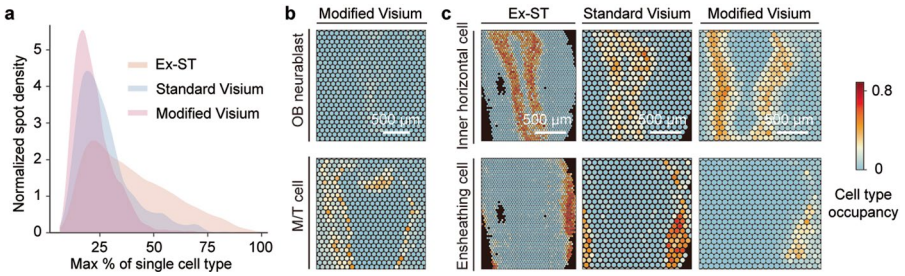

Extended Data Fig. 4 | Cell type compositions of spots in the MOB datasets. **a**, Density plot showing the distribution of dominating cell type occupancy at each spot for Ex-ST and Visium using standard and modified protocols. **b**, Cell type occupancy of each spot in the modified Visium data visualized for two cell types, OB neuroblasts and M/T cells. **c**, Comparison of cell type composition at individual spots in the Ex-ST, standard Visium, and modified Visium datasets visualized for two cell types, inner horizontal cells located in GCL and ensheathing cells in ONL.

https://doi.org/10.1038/s41592-023-01911-1

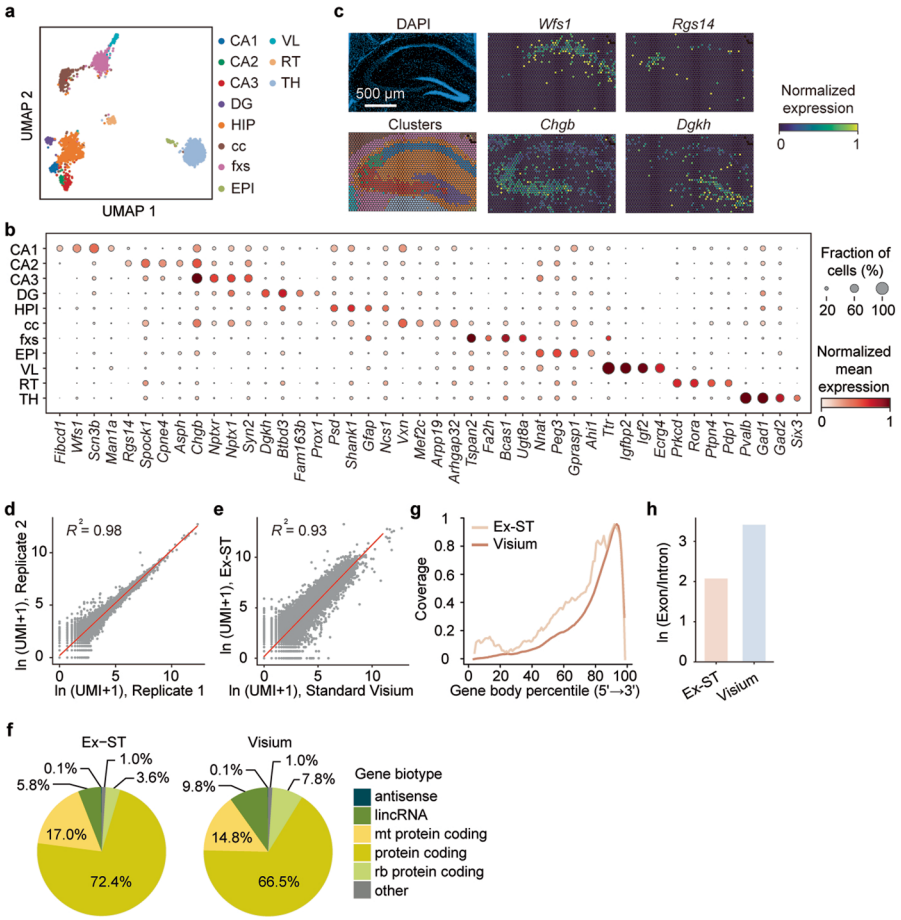

Extended Data Fig. 5 | Characterization of the Ex-ST mouse hippocampus data. a, UMAP showing the annotated clusters identified by unsupervised clustering of the Ex-ST hippocampus data. **b**, Dot plot showing the top marker genes of each cluster. **c**, Spatial gene expression of region-specific marker genes measured by Ex-ST, that is, *Wfs* for CA1, *Rgs14* for CA2, *Chgb* for CA3, *Dgkh* for DG. **d**, Comparison of the number UMIs per gene between the Ex-ST replicates. **e**, Comparison of the number of UMIs per gene in the Ex-ST and standard Visium datasets. **f**, Pie charts showing RNA biotype composition in the Ex-ST and standard Visium data. Proportions are quantified by the UMI counts of each biotype. **g**, Gene body coverage of the Ex-ST and standard Visium data. **h**, Ratio of exonic and intronic reads in the Ex-ST and standard Visium datasets.

https://doi.org/10.1038/s41592-023-01911-1

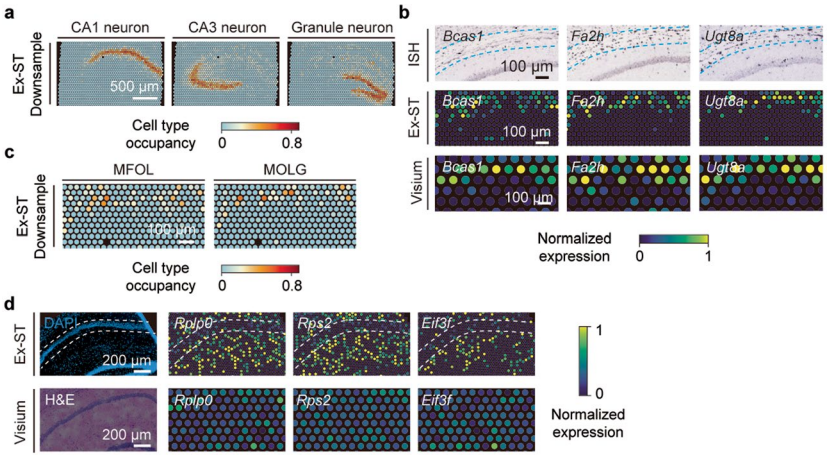

Extended Data Fig. 6 | Ex-ST hippocampal data has higher spatial resolution compared to standard Visium. a, Cell type composition of individual spots in the Ex-ST data downsampled to match the sequencing saturation of the 10x Genomics dataset. Three major neuronal cell types are shown. Note that the patterns are almost identical to Fig. 2b, suggesting that cell type devolution is mostly insensitive to sequencing depth in the regime of 60–90% saturation. **b**, Comparison of ISH (top), obtained from Allen Brain Atlas[10], normalized spatial expression of oligodendrocyte marker genes detected by Ex-ST (middle) and standard Visium (bottom). **c**, Cell type composition of individual spots in Ex-ST downsampled to match the sequencing saturation of the 10x Genomics data. Oligodendrocyte subclasses are shown, with patterns identical to Fig. 2e. **d**, Comparison of normalized spatial distribution of low-expression dendrite-enriched transcripts between Ex-ST and standard Visium. Note the lack of pattern in the standard Visium data.

https://doi.org/10.1038/s41592-023-01911-1

Extended Data Table 1 | Sample information obtained from space ranger software (10x Genomics) output

Sample name	Number of spots under tissue	Sequencing saturation	Mean reads per spot
Ex-ST_MOB_replicate_1	2 774	93.50%	33 591
Ex-ST_MOB_replicate_2	2 331	94.10%	35 598
Standard_Visium_MOB	1 301	91.70%	86 429
Ex-ST_MOB_replicate_1_downsampled	2 774	61.60%	3 605
Ex-ST_MOB_replicate_2_downsampled	2 331	61.80%	3 432
Standard_Visium_MOB_downsampled	1 301	57.20%	7 663
Modified_Visium_MOB_replicate_1	1 448	60.30%	249 532
Modified_Visium_MOB_replicate_2	1 490	57.40%	183 162
Ex-ST_Hippocampus_replicate_1	3 049	88.80%	25 660
Ex-ST_Hippocampus_replicate_2	3 191	89.00%	33 928
Standard Visium Hippocampus (10x Genomics dataset)	2 698	61.90%	115 740
Ex-ST_Hippocampus_replicate_1_downsampled	3 049	60.30%	4 395
Ex-ST_Hippocampus_replicate_2_downsampled	3 191	59.70%	5 659

Visium mouse olfactory bulb (MOB) datasets obtained using the standard and modified protocols were collected on tissue sections containing two bulbs. Both bulbs are combined to compare with the expanded MOB data with two replicates each containing one bulb. Downsampled Ex-ST and standard Visium MOB data have sequencing saturation matching with the data generated using the modified protocol. Hippocampus data include matched tissue areas from coronal sections of the mouse brain in the hippocampal region. Downsampled Ex-ST hippocampus data have sequencing saturation matching with the 10x Genomics hippocampus data. With matched sequencing saturation, the Ex-ST data always contain fewer reads per spot compared with the Visium datasets. This is expected given that each spot in the Ex-ST data corresponds to fewer cells and therefore should have lower library complexity.

https://doi.org/10.1038/s41592-023-01911-1

Extended Data Table 2 | Dendritically enriched gene list

Gene name	Detected by Ex-ST?	Detected by ST?	Detected by downsampled Ex-ST?	Detected by Joshua, et al.?	Detected by Tushev, et al.?	Detected by Slide_seq V2?
1700017B05Rik	Y	N	Y	Y		
2700081O15Rik	Y	N	Y	Y		
4930481A15Rik	Y	N	Y	Y		
Aaas	Y	N	Y	Y		
Abat	Y	N	Y			Y
Abcd1	Y	N	Y	Y		
Abcd2	Y	N	Y		Y	Y
Abhd4	Y	N	Y	Y		
Abl1	Y	N	Y	Y		
Acadm	Y	N	Y	Y		
Acat3	Y	N	Y	Y		
Acsf2	Y	N	Y		Y	
Acsl6	Y	N	Y	Y		Y
Adap1	Y	N	Y		Y	
Adarb1	Y	N	Y		Y	
Adarb2	Y	N	Y	Y		Y
Adcy1	Y	N	Y	Y		
Adcy5	Y	N	Y			Y
Adcyap1r1	Y	N	Y	Y	Y	
Afg3l1	Y	N	Y	Y		
Agap1	Y	N				Y
Agl	Y	N	Y	Y		
AI506816	Y	N	Y	Y		
Akt2	Y	N	Y	Y		
Aldh6a1	Y	N		Y		
Ankrd13a	Y	N	Y	Y		
Ankrd26	Y	N	Y	Y		
Ankrd40	Y	N		Y		
Anp32e	Y	N	Y	Y		
Ap3s2	Y	N	Y			Y
Apba1	Y	N	Y	Y		
Apod	Y	N	Y	Y		
Arhgap11a	Y	N			Y	
Arhgap30	Y	N	Y		Y	
Arhgap33	Y	N	Y	Y		
Arid3a	Y	N	Y	Y		
Arl3	Y	N	Y		Y	
Arl6ip6	Y	N	Y	Y		
Armcx6	Y	N	Y	Y		
Arnt2	Y	N	Y	Y	Y	
Arpc1b	Y	N	Y	Y		
Arpp21	Y	N	Y	Y		
Arrdc3	Y	N	Y	Y		
Arxes2	Y	N	Y	Y		
Asrgl1	Y	N	Y			Y
Atp1a2	Y	N	Y	Y		Y
Atr	Y	N	Y		Y	
Baalc	Y	N	Y			Y

 https://doi.org/10.1038/s41592-023-01911-1

Extended Data Table 2 | (contiunued) Dendritically enriched gene list

Bach2	Y	N	Y	Y		
Bak1	Y	N	Y	Y		
Bard1	Y	N	Y	Y		
Baz1a	Y	N	Y		Y	
BC030867	Y	N	Y	Y		
BC035044	Y	N	Y	Y		
Bcr	Y	N		Y		
Begain	Y	N	Y	Y		
Bloc1s1	Y	N	Y	Y		
Bola2	Y	N	Y	Y		
Brix1	Y	N	Y	Y		
Brpf3	Y	N	Y	Y		
Btbd3	Y	N	Y			Y
C030006K11Rik	Y	N	Y	Y		
Cbfa2t3	Y	N	Y			Y
Ccdc88a	Y	N	Y	Y		
Cd63	Y	N		Y		
Cd79b	Y	N			Y	
Cdc42ep1	Y	N	Y	Y		
Cdc42ep4	Y	N	Y	Y		
Cdk16	Y	N	Y	Y		Y
Cdk2ap1	Y	N	Y	Y		
Cep250	Y	N	Y	Y		
Cfh	Y	N	Y	Y		
Chaf1a	Y	N	Y	Y		
Chaf1b	Y	N			Y	
Chd3	Y	N	Y	Y		
Chmp1a	Y	N	Y	Y		
Chrna4	Y	N	Y	Y		Y
Cib2	Y	N	Y	Y		Y
Cic	Y	N	Y	Y		
Cit	Y	N	Y	Y		Y
Clic4	Y	N	Y	Y		
Clmn	Y	N	Y			Y
Clu	Y	N	Y			Y
Cnp	Y	N	Y	Y		
Cnpy3	Y	N	Y	Y		
Cnr1	Y	N	Y			Y
Cntfr	Y	N	Y	Y		
Coa7	Y	N	Y	Y		
Coil	Y	N	Y	Y		
Cox15	Y	N	Y	Y		
Cox7a2l	Y	N	Y	Y		
Cplx2	Y	N	Y			Y
Cpne3	Y	N	Y	Y		
Crip1	Y	N	Y	Y		
Crot	Y	N		Y		
Crtc1	Y	N	Y	Y		
Csdc2	Y	N				Y
Csrnp2	Y	N	Y	Y		
Ctnnbip1	Y	N	Y			Y
Ctnnd2	Y	N	Y	Y	Y	Y
Ctsz	Y	N	Y	Y		

 https://doi.org/10.1038/s41592-023-01911-1

Extended Data Table 2 | (contiunued) Dendritically enriched gene list

Cul4b	Y	N	Y	Y			
Cuta	Y	N	Y	Y			
Cux1	Y	N		Y			
Cyb5d1	Y	N	Y	Y			
D8Ertd738e	Y	N	Y	Y			Y
Dab2ip	Y	N	Y	Y			
Dad1	Y	N	Y	Y			
Dbndd1	Y	N	Y	Y			
Dbnl	Y	N	Y		Y		
Ddit4l	Y	N	Y	Y			
Dennd2a	Y	N	Y	Y			
Dgkeos	Y	N	Y	Y			
Dio2	Y	N					Y
Dlg2	Y	N	Y	Y			Y
Dlgap2	Y	N	Y	Y			
Dlgap3	Y	N	Y	Y			
Dmwd	Y	N	Y	Y			
Dnajc19	Y	N	Y	Y			
Dnajc2	Y	N	Y	Y			
Dnajc27	Y	N	Y	Y			
Dnm2	Y	N	Y	Y			
Dok6	Y	N	Y				Y
Dolpp1	Y	N	Y	Y			
Drap1	Y	N	Y	Y			Y
Dtl	Y	N	Y		Y		
Dtx3l	Y	N	Y	Y			
Dusp15	Y	N	Y				Y
Dusp16	Y	N	Y	Y			
Dyrk1b	Y	N	Y	Y			
Dzip1	Y	N	Y	Y			
E130114P18Rik	Y	N	Y	Y			
E2f1	Y	N	Y	Y			
E2f2	Y	N			Y		
Edem1	Y	N	Y	Y			
Eef1b2	Y	N	Y	Y			
Eif2d	Y	N	Y	Y			
Eif3f	Y	N	Y	Y			
Eif3h	Y	N	Y	Y			
Eif3j1	Y	N	Y	Y			
Eif4ebp2	Y	N	Y	Y			
Enho	Y	N	Y	Y			
Enpp2	Y	N	Y	Y			
Epas1	Y	N	Y	Y			Y
Epb41l1	Y	N	Y				Y
Epn1	Y	N	Y	Y	Y		
Eps8	Y	N		Y			
Evi5l	Y	N	Y	Y			
Ezh2	Y	N	Y	Y			
Ezr	Y	N	Y	Y			
Fam102a	Y	N	Y	Y			
Fam111a	Y	N	Y	Y			
Fam149b	Y	N	Y	Y			
Fam163a	Y	N	Y		Y		Y

https://doi.org/10.1038/s41592-023-01911-1

Extended Data Table 2 | (contiunued) Dendritically enriched gene list

Fam177a	Y	N	Y		Y	
Fam184a	Y	N	Y	Y		
Fasn	Y	N	Y		Y	
Fat1	Y	N	Y	Y		
Fbl	Y	N	Y	Y		
Fbxo41	Y	N	Y	Y		Y
Fgd2	Y	N	Y	Y		
Fgf1	Y	N	Y	Y		
Fgf11	Y	N	Y	Y		
Fgf13	Y	N	Y	Y		Y
Fkbp2	Y	N	Y	Y	Y	
Fmn1	Y	N	Y	Y		
Fmn2	Y	N	Y	Y		
Fosb	Y	N	Y			Y
Foxo3	Y	N	Y	Y		
Ftl1	Y	N	Y	Y		
Fxyd1	Y	N	Y	Y		Y
G6pc3	Y	N	Y	Y		
Gabrg1	Y	N	Y	Y	Y	
Gad2	Y	N	Y	Y	Y	
Galk1	Y	N	Y	Y		
Gas2l1	Y	N	Y	Y		
Gas6	Y	N	Y	Y		
Gas8	Y	N	Y	Y		
Gatm	Y	N	Y	Y		
Gcsh	Y	N	Y		Y	
Gdf11	Y	N	Y	Y		
Gdpd2	Y	N	Y	Y		
Gfod1	Y	N	Y			Y
Glb1	Y	N	Y	Y		
Gmpr2	Y	N	Y	Y		
Gna12	Y	N	Y			Y
Gnai2	Y	N	Y	Y		
Gng13	Y	N	Y			Y
Gng7	Y	N	Y	Y	Y	Y
Golga7b	Y	N	Y			Y
Gp1bb	Y	N	Y	Y		
Gpld1	Y	N	Y	Y		
Gpt	Y	N	Y	Y		
Grm3	Y	N	Y	Y		Y
Grm8	Y	N	Y	Y		
Gstm5	Y	N	Y	Y		
Gtf2e2	Y	N	Y	Y		
H2-D1	Y	N	Y	Y		
Hapln1	Y	N	Y		Y	Y
Hck	Y	N			Y	
Hdac5	Y	N	Y	Y		
Hells	Y	N	Y	Y		
Hemk1	Y	N	Y			Y
Hinfp	Y	N	Y	Y		
Hipk1	Y	N	Y	Y		
Hipk2	Y	N	Y		Y	
Hira	Y	N	Y	Y		

 https://doi.org/10.1038/s41592-023-01911-1

Extended Data Table 2 | (contiunued) Dendritically enriched gene list

Hist1h1b	Y	N			Y	
Hist1h1c	Y	N	Y	Y		
Hist1h1d	Y	N	Y		Y	
Hist1h2ac	Y	N	Y	Y		
Hist1h2ae	Y	N	Y	Y		
Hist1h2ap	Y	N			Y	
Hist1h2bc	Y	N	Y	Y		
Hmgb2	Y	N	Y	Y		
Hsd3b7	Y	N	Y	Y		
Hspb8	Y	N	Y	Y		
Id3	Y	N	Y	Y		
Id4	Y	N	Y	Y		
Idua	Y	N	Y	Y		
Ifi27	Y	N	Y	Y		
Igbp1	Y	N	Y	Y		
Igf2	Y	N	Y	Y		
Il33	Y	N		Y		
Il6st	Y	N	Y	Y		
Iqsec2	Y	N	Y	Y		
Iqsec3	Y	N	Y			Y
Irak1	Y	N	Y		Y	
Itpripl1	Y	N	Y		Y	
Jade1	Y	N	Y	Y		
Jagn1	Y	N	Y	Y		
Jph3	Y	N	Y			Y
Kcnj13	Y	N	Y		Y	
Kdm6b	Y	N	Y	Y		
Kif1c	Y	N	Y	Y		
Kifc2	Y	N	Y	Y		
Kirrel2	Y	N	Y		Y	
Kiss1r	Y	N	Y	Y		
Lamp2	Y	N	Y	Y		
Lars2	Y	N	Y	Y		
Lbr	Y	N	Y	Y		
Lca5	Y	N	Y	Y		
Limch1	Y	N	Y	Y		
Lims1	Y	N	Y	Y		
Litaf	Y	N	Y	Y		
Lix1	Y	N	Y			Y
Lrch4	Y	N	Y	Y		
Lrp10	Y	N	Y	Y		
Ltbp1	Y	N	Y		Y	
Ly86	Y	N	Y	Y		
Mafg	Y	N	Y		Y	Y
Malat1	Y	N	Y	Y		
Map3k10	Y	N	Y	Y		
Marf1	Y	N	Y	Y		
Mars	Y	N	Y	Y		
Mbp	Y	N	Y	Y		
Mcl1	Y	N	Y	Y		
Med25	Y	N	Y	Y		
Mef2c	Y	N	Y		Y	
Meis2	Y	N	Y	Y		

 https://doi.org/10.1038/s41592-023-01911-1

Extended Data Table 2 | (contiunued) Dendritically enriched gene list

Mfap1b	Y	N	Y	Y		
Mfap3l	Y	N	Y			Y
Mfge8	Y	N	Y		Y	
Mgat4b	Y	N	Y	Y		
Mgll	Y	N	Y	Y		Y
Mgmt	Y	N	Y	Y		
Mlst8	Y	N	Y	Y		
Mmp24	Y	N	Y			Y
Mn1	Y	N	Y	Y		
Mob1a	Y	N	Y	Y		
Mospd2	Y	N	Y	Y		
Mospd3	Y	N	Y	Y		Y
Mpdu1	Y	N	Y	Y		
Mpst	Y	N	Y	Y		
Mrc1	Y	N		Y		
Mreg	Y	N	Y	Y		
Msn	Y	N	Y	Y		
Mt3	Y	N	Y		Y	Y
mt-Atp6	Y	N	Y	Y		
Mturn	Y	N	Y	Y	Y	
Mvb12a	Y	N	Y	Y		
Mycbp	Y	N	Y	Y		
Myh9	Y	N	Y	Y		
Nadk2	Y	N	Y	Y		
Nckap5	Y	N	Y	Y		
Ndrg1	Y	N	Y	Y		
Nenf	Y	N	Y	Y		
Nf2	Y	N	Y			Y
Nfkb2	Y	N	Y	Y		
Nme2	Y	N	Y	Y		
Nmral1	Y	N	Y	Y		
Nop2	Y	N	Y	Y		
Npc2	Y	N	Y	Y		
Nr2e1	Y	N	Y		Y	
Nsdhl	Y	N	Y	Y		
Nudc	Y	N	Y	Y		
Nup133	Y	N	Y	Y		
Oat	Y	N	Y	Y		
Oxa1l	Y	N	Y	Y		
P2ry12	Y	N	Y	Y		
Pabpc1	Y	N	Y	Y		
Palm	Y	N	Y	Y		
Panx2	Y	N	Y			Y
Pcdhgc5	Y	N			Y	
Pcsk6	Y	N	Y	Y		
Pctp	Y	N		Y		
Pcyt1b	Y	N	Y		Y	
Pdxdc1	Y	N	Y	Y		Y
Pdxk	Y	N	Y	Y		Y
Pdzd4	Y	N	Y	Y		
Phactr1	Y	N	Y			Y
Phc1	Y	N	Y	Y		
Phyh	Y	N	Y	Y		Y

 https://doi.org/10.1038/s41592-023-01911-1

Extended Data Table 2 | (contiunued) Dendritically enriched gene list

Phyhipl	Y	N	Y	Y			
Pigq	Y	N	Y	Y			
Pigu	Y	N	Y	Y			
Pik3r1	Y	N	Y	Y			
Pink1	Y	N	Y	Y			
Pip5k1c	Y	N	Y		Y		
Pitpnm2	Y	N	Y	Y	Y		
Pknox1	Y	N	Y	Y			
Pla2g7	Y	N	Y	Y			
Plekhb2	Y	N	Y	Y			Y
Plekhm2	Y	N		Y			
Plk3	Y	N	Y	Y			
Plk4	Y	N	Y	Y			
Plxnb1	Y	N	Y	Y			
Pnp	Y	N	Y	Y			
Pom121	Y	N	Y		Y		
Pomgnt1	Y	N	Y	Y			
Ppfia3	Y	N	Y	Y			
Ppp1r16a	Y	N	Y	Y			
Prcp	Y	N	Y	Y			
Prex1	Y	N		Y			
Prkaa2	Y	N	Y	Y			
Prkcd	Y	N	Y	Y			
Prr11	Y	N			Y		
Prr13	Y	N	Y	Y			
Prrc2a	Y	N		Y			
Psd2	Y	N	Y	Y			
Psme1	Y	N	Y	Y			
Ptp4a3	Y	N	Y	Y			
Ptpmt1	Y	N	Y		Y		
Ptpn1	Y	N	Y	Y			
Pycr1	Y	N			Y		
Pygb	Y	N	Y	Y			
Qars	Y	N	Y	Y			
Qdpr	Y	N		Y			
Rab11fip4	Y	N	Y		Y		Y
Rack1	Y	N	Y				Y
Rapgef4	Y	N	Y	Y			
Rasa3	Y	N	Y	Y			
Rasl10b	Y	N	Y	Y			
Rbck1	Y	N	Y	Y			
Rcan3	Y	N	Y	Y			
Reep6	Y	N	Y	Y			
Reln	Y	N	Y		Y		
Rftn2	Y	N		Y			
Rgs20	Y	N		Y			
Rhog	Y	N	Y	Y			
Rhoh	Y	N	Y	Y			
Rin2	Y	N	Y	Y			
Rmst	Y	N	Y	Y			
Rnf165	Y	N	Y				Y
Rnf31	Y	N	Y	Y			
Rpia	Y	N	Y	Y			

 https://doi.org/10.1038/s41592-023-01911-1

Extended Data Table 2 | (contiunued) Dendritically enriched gene list

Rpl27	Y	N	Y	Y			
Rplp0	Y	N	Y	Y			
Rps12	Y	N	Y	Y			
Rps13	Y	N	Y	Y			
Rps16	Y	N	Y	Y			
Rps2	Y	N	Y	Y			
Rps6ka4	Y	N	Y		Y		
Rsu1	Y	N	Y	Y			
Rtn2	Y	N	Y	Y			
Ryk	Y	N	Y	Y			
Samd4	Y	N	Y	Y			
Sbk1	Y	N	Y	Y			Y
Scaf1	Y	N		Y			
Scd1	Y	N	Y	Y			
Scd3	Y	N	Y	Y			
Scrt1	Y	N	Y				Y
Sdhc	Y	N	Y	Y			
Sec61a1	Y	N	Y	Y			
Serinc3	Y	N	Y	Y			
Serpine2	Y	N	Y	Y			
Setd3	Y	N	Y	Y			
Sft2d2	Y	N	Y	Y			
Sfxn1	Y	N	Y	Y			
Sgsm2	Y	N	Y	Y			
Sh2b1	Y	N	Y	Y			
Sh3glb1	Y	N	Y	Y			Y
Shank1	Y	N	Y				Y
Shank3	Y	N	Y				Y
Shc3	Y	N			Y		Y
Shisa4	Y	N		Y			
Sipa1l1	Y	N	Y				Y
Ski	Y	N	Y	Y			
Slamf9	Y	N			Y		
Slc12a2	Y	N	Y	Y			
Slc1a2	Y	N	Y	Y			Y
Slc1a3	Y	N	Y	Y			Y
Slc25a33	Y	N	Y	Y			
Slc38a3	Y	N	Y				Y
Slc6a1	Y	N	Y	Y	Y		Y
Slc6a11	Y	N	Y				Y
Slc6a8	Y	N	Y	Y			
Slpi	Y	N		Y			
Smarcal1	Y	N	Y	Y			
Smarcc2	Y	N	Y	Y			Y
Smdt1	Y	N	Y		Y		Y
Smpdl3a	Y	N	Y	Y			
Snx9	Y	N	Y	Y			
Socs7	Y	N	Y	Y			
Sord	Y	N	Y	Y			
Spata13	Y	N	Y	Y			
Srcin1	Y	N	Y				Y
Srf	Y	N	Y	Y			
Stat3	Y	N	Y	Y			

 https://doi.org/10.1038/s41592-023-01911-1

Extended Data Table 2 | (contiunued) Dendritically enriched gene list

Stk17b	Y	N	Y	Y		
Stk40	Y	N	Y	Y		
Stpg1	Y	N	Y	Y		
Stxbp5l	Y	N	Y		Y	
Suds3	Y	N	Y	Y		Y
Swap70	Y	N	Y	Y		
Syf2	Y	N	Y	Y		
Syn3	Y	N	Y	Y		
Taf9	Y	N	Y	Y		
Tbccd1	Y	N	Y	Y		
Tbkbp1	Y	N	Y			Y
Tdp1	Y	N	Y	Y		
Tdrd3	Y	N	Y	Y		
Tef	Y	N	Y		Y	
Thra	Y	N	Y	Y		Y
Tmem134	Y	N	Y	Y		
Tmem151b	Y	N	Y	Y		
Tmem160	Y	N	Y		Y	
Tmem185b	Y	N	Y	Y		
Tmem229a	Y	N	Y			Y
Tmpo	Y	N	Y	Y		
Tnfaip8l2	Y	N	Y	Y		
Tnrc18	Y	N	Y	Y		
Tor1aip1	Y	N	Y	Y		
Tprkb	Y	N	Y	Y		
Trak1	Y	N	Y	Y		
Trim12a	Y	N	Y	Y		
Trim12c	Y	N	Y	Y		
Trim59	Y	N	Y	Y		
Trmt112	Y	N	Y	Y		
Trp53bp2	Y	N	Y	Y		
Trp53inp1	Y	N	Y	Y		
Tsen34	Y	N	Y	Y		
Ttc7b	Y	N	Y	Y		
Ttf1	Y	N	Y	Y		
Ttll3	Y	N	Y	Y		
Ttr	Y	N	Y		Y	
Tuba1c	Y	N	Y	Y		
Txnip	Y	N	Y	Y		
U2af1l4	Y	N	Y	Y		
Ubqln4	Y	N	Y	Y		Y
Ubxn7	Y	N	Y	Y		
Ucp2	Y	N	Y	Y		
Uqcr11	Y	N	Y	Y		Y
Usp21	Y	N	Y	Y		
Usp6nl	Y	N	Y	Y		
Vip	Y	N	Y		Y	
Wbp1	Y	N	Y	Y		
Wdr44	Y	N	Y	Y		
Wdr89	Y	N	Y	Y		
Wiz	Y	N	Y			Y
Xrcc5	Y	N	Y	Y		
Ybx1	Y	N	Y	Y	Y	

https://doi.org/10.1038/s41592-023-01911-1

Extended Data Table 2 | (contiunued) Dendritically enriched gene list

Yes1	Y	N	Y	Y	
Zadh2	Y	N	Y	Y	
Zbtb14	Y	N	Y	Y	
Zfp146	Y	N	Y		Y
Zfp341	Y	N	Y	Y	
Zfp358	Y	N	Y	Y	
Zfp366	Y	N			Y
Zfp367	Y	N	Y	Y	
Zfp568	Y	N	Y	Y	
Zfp574	Y	N	Y	Y	
Zfp664	Y	N	Y	Y	
Zfp703	Y	N	Y	Y	
Zfp867	Y	N	Y	Y	
Zmiz2	Y	N	Y	Y	

Dendrite-enriched transcripts detected by Ex-ST but unresolvable using the standard Visium protocol are listed. Also provided are the previous measurements[18–20] that support the dendritic expression of these transcripts and whether these transcripts are detected in the downsampled Ex-ST data.

nature portfolio

Corresponding author(s): Bo Wang, Joakim Lundeberg

Last updated by author(s): Apr 20, 2023

Reporting Summary

Nature Portfolio wishes to improve the reproducibility of the work that we publish. This form provides structure for consistency and transparency in reporting. For further information on Nature Portfolio policies, see our Editorial Policies and the Editorial Policy Checklist.

Statistics

For all statistical analyses, confirm that the following items are present in the figure legend, table legend, main text, or Methods section.

n/a	Confirmed	
☐	☒	The exact sample size (*n*) for each experimental group/condition, given as a discrete number and unit of measurement
☐	☒	A statement on whether measurements were taken from distinct samples or whether the same sample was measured repeatedly
☐	☒	The statistical test(s) used AND whether they are one- or two-sided *Only common tests should be described solely by name; describe more complex techniques in the Methods section.*
☒	☐	A description of all covariates tested
☒	☐	A description of any assumptions or corrections, such as tests of normality and adjustment for multiple comparisons
☐	☒	A full description of the statistical parameters including central tendency (e.g. means) or other basic estimates (e.g. regression coefficient) AND variation (e.g. standard deviation) or associated estimates of uncertainty (e.g. confidence intervals)
☐	☒	For null hypothesis testing, the test statistic (e.g. *F*, *t*, *r*) with confidence intervals, effect sizes, degrees of freedom and *P* value noted *Give P values as exact values whenever suitable.*
☒	☐	For Bayesian analysis, information on the choice of priors and Markov chain Monte Carlo settings
☒	☐	For hierarchical and complex designs, identification of the appropriate level for tests and full reporting of outcomes
☒	☐	Estimates of effect sizes (e.g. Cohen's *d*, Pearson's *r*), indicating how they were calculated

Our web collection on statistics for biologists contains articles on many of the points above.

Software and code

Policy information about availability of computer code

Data collection	Zen Pro 2012, space ranger (version 1.0.0 for standard Visium data, and version 1.3.0 adapted with custom barcode list for Ex-ST data, 10x Genomics).
Data analysis	Python (version 3.7.12), R (version 4.0.5), Seqtk (version 1.3), Loupe Browser (v 4.0.0, 10x Genomics), Scanpy (version 1.8.2), SAM (version 0.8.9), Seurat (version 4.1.1), STUtility (version 0.1.0), sciPy (version 1.9.1). Custom code used for data analysis and generating figures is available at https://github.com/fyh1221/Expansion_Spatial_Transcriptomics.

For manuscripts utilizing custom algorithms or software that are central to the research but not yet described in published literature, software must be made available to editors and reviewers. We strongly encourage code deposition in a community repository (e.g. GitHub). See the Nature Portfolio guidelines for submitting code & software for further information.

Data

Policy information about availability of data

All manuscripts must include a data availability statement. This statement should provide the following information, where applicable:

- Accession codes, unique identifiers, or web links for publicly available datasets
- A description of any restrictions on data availability
- For clinical datasets or third party data, please ensure that the statement adheres to our policy

Mouse brain section containing hippocampus region is a publicly available dataset that can be found along with mouse reference genome mm10 on 10x Genomics

website (https://www.10xgenomics.com/resources/datasets/mouse-brain-section-coronal-1-standard-1-0-0). Single-cell RNAseq dataset of mouse brain can be downloaded online (http://mousebrain.org/adolescent/downloads.html). MOB bulk RNAseq and Slide-seq datasets used for comparison were obtained from references indicated in the paper. All data generated in this study (standard Visium data on MOB, all Ex-ST data, and Visium data generated using the modified protocol) including space ranger output files, stereoscope output files, DAPI and brightfield images are available at the Mendeley repository (http://dx.doi.org/10.17632/nrbsxrk9mp.1). Raw sequence data can be found at NCBI BioProject with accession number PRJNA957091.

Human research participants

Policy information about studies involving human research participants and Sex and Gender in Research.

Reporting on sex and gender	N.A.
Population characteristics	N.A.
Recruitment	N.A.
Ethics oversight	N.A.

Note that full information on the approval of the study protocol must also be provided in the manuscript.

Field-specific reporting

Please select the one below that is the best fit for your research. If you are not sure, read the appropriate sections before making your selection.

☒ Life sciences ☐ Behavioural & social sciences ☐ Ecological, evolutionary & environmental sciences

For a reference copy of the document with all sections, see nature.com/documents/nr-reporting-summary-flat.pdf

Life sciences study design

All studies must disclose on these points even when the disclosure is negative.

Sample size	Samples sizes were chosen based on previous studies of similar methodologies: Ståhl et al., Science, 2016; Vickovic et al., Nature Methods, 2019.
Data exclusions	No data was excluded from the analysis.
Replication	All experimental findings were repeated in independent biological replicates. This information is extensively described in the methods and figure captions, and the reproducibility between replicates is reported in Extended Data Figure 2 & 5.
Randomization	Animals were randomly selected from a large cohort for experiments. Randomization of animals was not relevant in our study, as it did not involve experiment/control groups of animals, and there was no comparison between animals .
Blinding	When comparing Ex-ST and ST results, researchers could not be blinded because sequencing data quality and resolution were obviously different. Blinding was not relevant to the study since all comparisons made between methods, including resolution, capture efficiency and gene expression, are highly objective and quantitive.

Reporting for specific materials, systems and methods

We require information from authors about some types of materials, experimental systems and methods used in many studies. Here, indicate whether each material, system or method listed is relevant to your study. If you are not sure if a list item applies to your research, read the appropriate section before selecting a response.

Materials & experimental systems

n/a	Involved in the study
☒	☐ Antibodies
☒	☐ Eukaryotic cell lines
☒	☐ Palaeontology and archaeology
☐	☒ Animals and other organisms
☒	☐ Clinical data
☒	☐ Dual use research of concern

Methods

n/a	Involved in the study
☒	☐ ChIP-seq
☒	☐ Flow cytometry
☒	☐ MRI-based neuroimaging

Animals and other research organisms

Policy information about studies involving animals; ARRIVE guidelines recommended for reporting animal research, and Sex and Gender in Research

Laboratory animals	Adult male CD1 mice (3-6 months old, Charles River) were used for the Ex-ST experiments. Animal procedures were approved by the Stanford University Animal Care and Use Committee and were in accordance with NIH guidelines. Animals were maintained with 12-hour light-dark cycle, with ambient temperature between 71-74 °F, humidity between 20-45 %, and provided with food and water ad libitum.
Wild animals	This study did not involve wild animals.
Reporting on sex	Male mice were used for this study. Neural structures investigated in this study were found in both sexes (Luo, Principles of neurobiology, 2020).
Field-collected samples	This study did not involve field-collected samples.
Ethics oversight	Animal procedures were approved by the Stanford University Animal Care and Use Committee and were in accordance with NIH guidelines. Mouse olfactory bulb samples for standard Visium experiment were commercially purchased from Adlego Biomedical, which operates under ethical permission nr. 17114-2020.

Note that full information on the approval of the study protocol must also be provided in the manuscript.